AIAA JOURNAL
Vol. 45, No. 11, November 2007

Effects of Leading-Edge Protuberances on Airfoil Performance

H. Johari*
Worcester Polytechnic Institute, Worcester, Massachusetts 01609
C. Henoch†
Naval Undersea Warfare Center, Newport, Rhode Island 02841
and
D. Custodio‡ and A. Levshin‡
Worcester Polytechnic Institute, Worcester, Massachusetts 01609

DOI: 10.2514/1.28497

Lift, drag, and pitching moments of airfoils with leading-edge sinusoidal protuberances were measured in a water tunnel and compared with those of a baseline 63_4-021 airfoil. The amplitude of the leading-edge protuberances ranged from 2.5 to 12% of the mean chord length; the spanwise wavelengths were 25 and 50% of the mean chord length. These ranges correspond to the morphology found on the leading edge of humpback whales' flippers. Flow visualization using tufts was also performed to examine the separation characteristics of the airfoils. For angles of attack less than the baseline stall angle, lift reduction and drag increase were observed for the modified foils. Above this angle, lift of the modified foils was up to 50% greater than the baseline foil with little or no drag penalty. The amplitude of the protuberances had a distinct effect on the performance of the airfoils, whereas the wavelength had little. Flow visualization indicated separated flow originating primarily from the troughs and attached flow on the peaks of the protuberances at angles beyond the stall angle of the baseline foil.

Nomenclature

C_d	=	drag coefficient, $2D/\rho U_\infty^2 sc$
C_l	=	lift coefficient, $2L/\rho U_\infty^2 sc$
C_m	=	pitching moment coefficient, $2M/\rho U_\infty^2 sc^2$
c	=	mean chord length
D	=	drag force
L	=	lift force
M	=	pitching moment
Re	=	Reynolds number, $U_\infty c/\nu$
s	=	span
U_∞	=	freestream velocity
α	=	angle of attack
ν	=	kinematic viscosity
ρ	=	density

I. Introduction

THE idea of examining the effects of leading-edge protuberances on airfoil performance was inspired by previous work of marine biologists who studied the morphology of humpback whales' pectoral flippers. Despite its large size and rigid body, the humpback whale (*Megaptera novaeangliae*) is extremely maneuverable compared with other species. Turning maneuvers are especially evident during pursuit of prey. The agility of the humpback whale has been attributed to its use of pectoral flippers [1,2]. Typical humpback whale flippers are shown in Fig. 1.

Fish and Battle [1] report that the flippers have large aspect ratios ($\approx$6), and large-scale protuberances are present on the leading edge. The flipper has a symmetric profile for the most part, with a rounded leading edge and a sharp trailing edge. The flipper thickness ratio ranges from 0.20 to 0.28 of the chord length, with a mean value of $0.23c$. The thickness ratio decreases from midspan to the tip. The maximum thickness point varies from about $0.2c$ at midspan to about $0.4c$ near the tip. The cross section of the flipper has a profile similar to a NACA 63_4-021 airfoil [1]. A cross section of the flipper is compared with a NACA 63_4-021 airfoil in Fig. 2. The amplitude of leading-edge protuberances ranges from 2.5 to 12% of the chord, with a spanwise extent of 10–50% of the chord depending on the location along the span. It has been hypothesized that the "bumpy" leading edge is used for flow control [1] and/or drag reduction [3].

Watts and Fish [4] examined the performance of a low aspect ratio wing with leading-edge protuberances numerically using panel methods and showed that at an angle of attack $\alpha = 10$ deg the lift increases by 4.8% over the baseline wing. Subsequently, Miklosovic et al. [5] investigated the lift and drag of humpback whale flipper models in a wind tunnel. Their study considered tapered wings with an aspect ratio approximating that of a whale flipper. They reported an increase over the baseline of maximum lift by 6% and a delay of stall angle of attack by about 40% for the flipper model with the protuberances. More recently, Stein and Murray [6] reported that a two-dimensional airfoil with a protuberance amplitude and period equal to the average value for the humpback whale flipper results in a significant loss of lift and an increase in drag for angles of attack between 8 and 12 deg. No data past 12 deg was reported in [6]. The difference between the airfoil study of Stein and Murray [6] and the others noted is that the earlier work tested finite wings and flipper models whose spanwise flow may have been affected by the presence of the leading-edge protuberances. The effects of leading-edge protuberances on sweptback whale flipper models have also been investigated experimentally by Murray et al. [7]. They reported enhanced aerodynamic performance with increasing sweep angle.

Superposition of three-dimensional disturbances on nominally two-dimensional bluff bodies has long been known to alter the regular vortex shedding and drag characteristics [8–12]. For example, Tanner [9] has reported drag reductions of over 60% for blunt wings with segmented trailing edges. The drag reduction associated with the three-dimensionality of bluff bodies stems from the resulting waviness of the separation line. For the foils considered in the current study, the introduction of the protuberances on the leading edge altered the entire flowfield over the foil, and was expected to have different effects than the previously observed drag reductions.

Presented as Paper 2868 at the 36th AIAA Fluid Dynamics Conference and Exhibit, San Francisco, CA, 5–8 June 2006; received 23 October 2006; revision received 12 June 2007; accepted for publication 2 July 2007.

*Professor, Mechanical Engineering Department; currently at California State University, Northridge. Associate Fellow AIAA.
†Research Engineer, Hydrodynamics Branch, Code 8233.
‡Graduate Research Assistant, Mechanical Engineering Department.

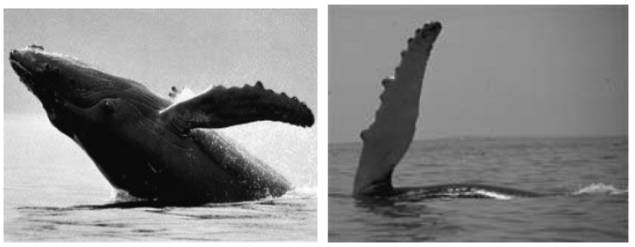

Fig. 1 Humpback whales' pectoral flippers. The large scale protuberances on the leading edge are shown.

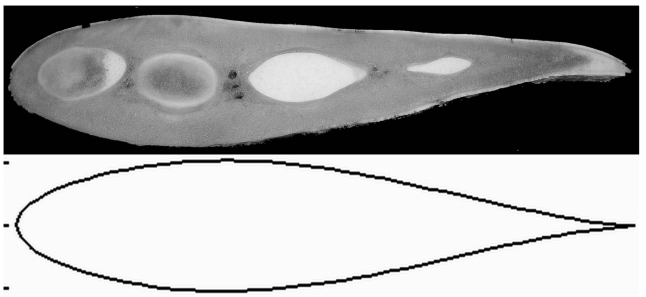

Fig. 2 Comparison of a humpback whale pectoral flipper cross section with the NACA 63_4-021 profile.

The primary objective of this experimental study is to investigate the aerodynamic loading resulting from the presence of leading-edge protuberances on a NACA 63_4-021 airfoil having a range of protuberance amplitudes and spanwise wavelengths. This study focused on the steady flow over two-dimensional airfoils with leading-edge protuberances to examine the fundamental nature of the resulting flow from the presence of protuberances. Forces and moments on the airfoil models were measured over a broad range of angle of attack ($-6 \leq \alpha \leq 30$ deg) in a water tunnel. Flow visualization using surface tufts was carried out to assess the effects of protuberances on the flowfield near the surface and the separated regions over the entire airfoils.

II. Experimental Technique

Two sets of rectangular aluminum airfoils based on the NACA 63_4-021 profile were machined and anodized. The mean chord length for the first set of seven airfoils was $c = 102$ mm and the span was $s = 203$ mm. One of the airfoils had a smooth leading edge and was used as the baseline airfoil for comparisons. The leading edge of the other six airfoils was sinusoidal in the spanwise direction, and the geometry was defined by a wavelength and amplitude. Three amplitudes of $0.025c$, $0.05c$, and $0.12c$ were chosen with two wavelengths of $0.25c$ and $0.50c$. The planform area for all airfoils in this set was equal to the smooth leading-edge baseline airfoil. All of the airfoils with the leading-edge protuberances in this set are shown in Fig. 3. The chosen relative amplitudes and the two wavelengths of the protuberances on the models in the present study fall within the range of values associated with the humpback whale flippers.

A second set of the airfoils was machined with a span of $s = 305$ mm and a mean chord length of $c = 102$ mm. This set, consisting of a baseline and three foils with leading-edge protuberances, was used for flow visualization and spanned the entire tunnel height. Tufts of 19 mm long yarn were attached to the airfoil surface to visualize the flow direction and condition near the surface. Regions of flow reversal and separation on the foils could be clearly discerned from still images and movies obtained during testing.

The experiments were carried out in the Naval Undersea Warfare Center (NUWC), Newport, Rhode Island water tunnel which has a 0.30 m square cross section. The freestream velocity was monitored at a point $6.5c$ upstream of the airfoils using a fiber optic laser

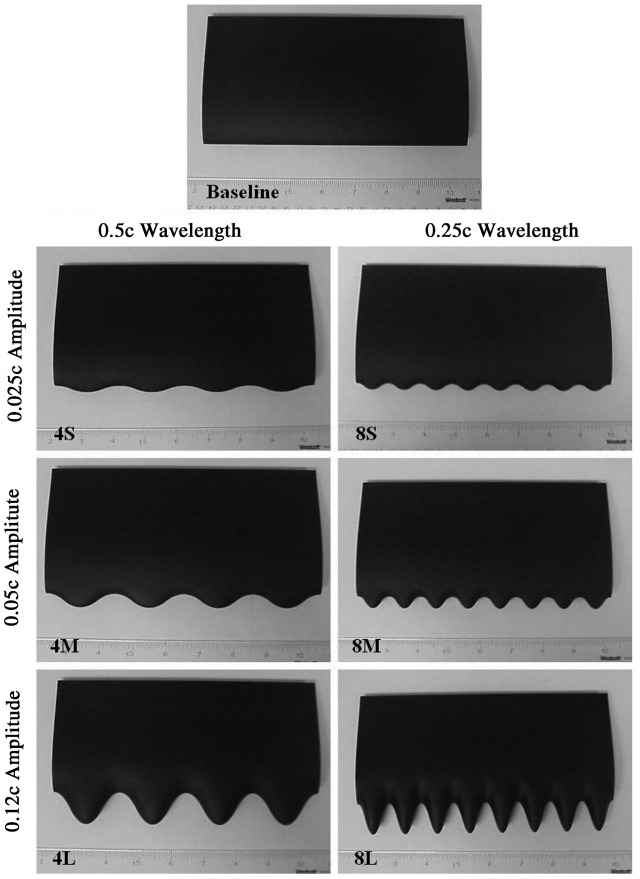

Fig. 3 Photographs of the baseline and modified airfoils with leading-edge protuberances.

Doppler velocimetry (LDV) system, and the measurements were taken at three speeds of $U_\infty = 1.0$, 1.4, and 1.8 m/s. Only the data for the highest freestream velocity of $U_\infty = 1.8$ m/s are reported here. The Reynolds number based on this freestream velocity and the mean chord length was $Re = 1.83 \times 10^5$ for all the data herein. For these tests, a pitch–yaw mechanism capable of precise angle-of-attack settings was employed. The forces and moments on the 203-mm-span airfoils were measured by a six-component waterproof load cell integrated within the pitch–yaw mechanism. The airfoils were fitted vertically between the tunnel ceiling and a fence to create a nominally two-dimensional section. The fence was attached to the airfoils and its drag contribution was measured separately and subtracted from the measured airfoil drag. Measurements of the forces and moments on the airfoils were conducted as a function of angle of attack over the range of $-6 \leq \alpha \leq 30$ deg. The measured data were converted to lift, drag, and pitching moment coefficients using the freestream dynamic pressure and the planform area. The latter was constant for the airfoils within the first set. The dimensionless coefficients were corrected for the solid and wake blockage by methods outlined in Pope and Ray [13].

The load cell in the setup has an uncertainty of 0.04 N for the lift and drag forces, and 0.001 N · m for the pitching moment. These values, along with the uncertainties in the freestream velocity and airfoil dimensions, translate to relative uncertainties of less than 1% for the lift and drag coefficients, and 3% for the moment coefficient. The estimated uncertainty for the angle of attack is 0.2 deg. The force coefficient uncertainties are smaller than the 5–7% rms fluctuations measured at angles of attack before the maximum lift.

III. Results

The measured lift, drag, and pitching moments for the baseline and foils with leading-edge protuberances are presented next. Flow visualization of selected foils at certain angles of attack is discussed subsequently. The foil designations and in the plots refer to those

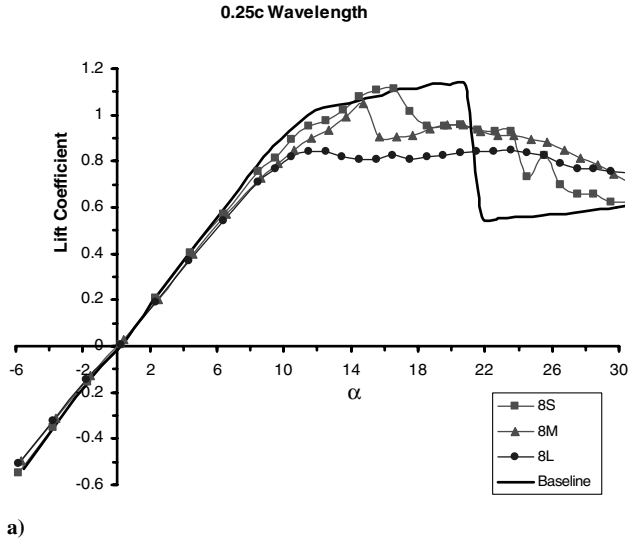

a)

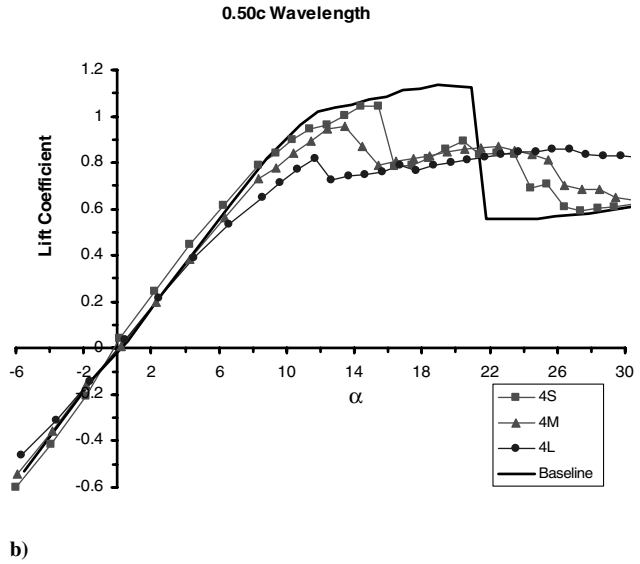

b)

Fig. 4 Lift coefficient variation with angle of attack.

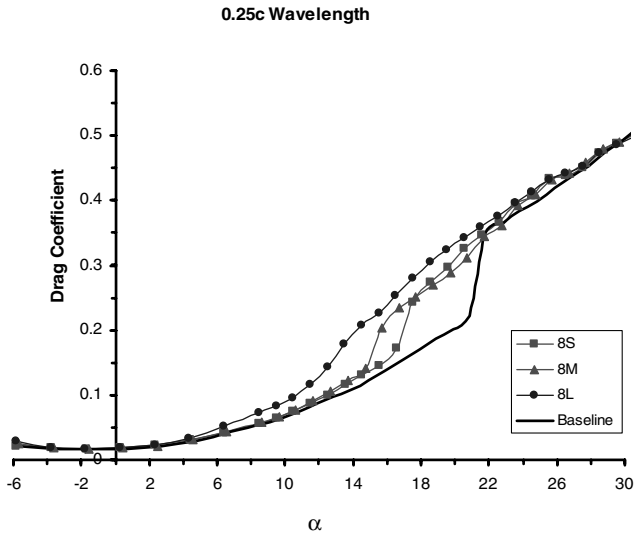

a)

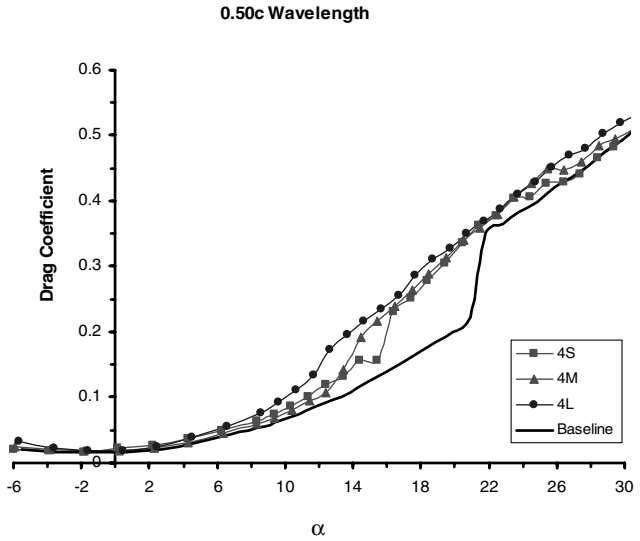

b)

Fig. 5 Drag coefficient variation with angle of attack.

indicated in Fig. 3; specifically, the first number refers to the wavelength (4 for $0.5c$ and 8 for $0.25c$) and the second character refers to the amplitude (S, M, and L for $0.025c$, $0.05c$, and $0.12c$) of the leading-edge protuberances.

A. Effect of Amplitude

The lift coefficient C_l for all of the airfoils is plotted in Fig. 4 as a function of angle of attack. The data for the shorter wavelength ($0.25c$) foils are compared with the baseline in Fig. 4a and those for the longer wavelength ($0.50c$) foils in Fig. 4b. The lift coefficient increases linearly with α for all airfoils up to about 8 deg.

The baseline foil C_l keeps increasing at a reduced rate up to $\alpha \approx 21$ deg, beyond which it stalls. The maximum C_l of 1.13 is reached at this angle of attack. The poststall C_l is nearly constant at 0.57 for $22 \leq \alpha \leq 28$ deg. The lift coefficient for the foil with the smallest leading-edge protuberances (8S) follows the baseline up to $\alpha \approx 17$ deg, and then drops to an intermediate plateau at $C_l \approx 0.94$. For $\alpha > 24$ deg, the C_l for this foil gets reduced to the value for the stalled baseline foil. The 8S foil has a much softer stall characteristic than the baseline foil. The data for the foil with the largest leading-edge protuberances (8L) are quite different. Once the C_l breaks from its linear rise, the lift coefficient remains constant at 0.82 for the range of $10 < \alpha < 26$ deg. This C_l value is 28% less than the $C_{l\max}$ for the baseline foil, but over 40% greater than the poststall C_l of the baseline. In essence, this airfoil (8L) does not stall in the traditional sense of a rapid decrease of C_l from a maximum value. The lift behavior for the foil with the intermediate leading-edge protuberance

Table 1 Aerodynamic characteristics of the airfoils

Airfoil	$dC_L/d\alpha$, per deg	$C_{l\max}$	α at $C_{l\max}$, deg	$C_{D\min}$	$L/D_{\max}$	α at $L/D_{\max}$, deg	Stall α, deg
Baseline	0.094	1.13	20.9	0.016	14.8	8.8	20.9
8S	0.091	1.12	16.5	0.019	13.6	6.4	16.5
8M	0.086	1.05	14.7	0.018	13.1	6.58	14.7
8L	0.085	0.85	23.5	0.018	11.2	4.4	——
4S	0.099	1.05	14.4	0.022	12.3	6.3	15.4
4M	0.090	0.96	13.4	0.019	12.5	6.3	13.4
4L	0.081	0.86	26.7	0.019	10.2	4.5	——

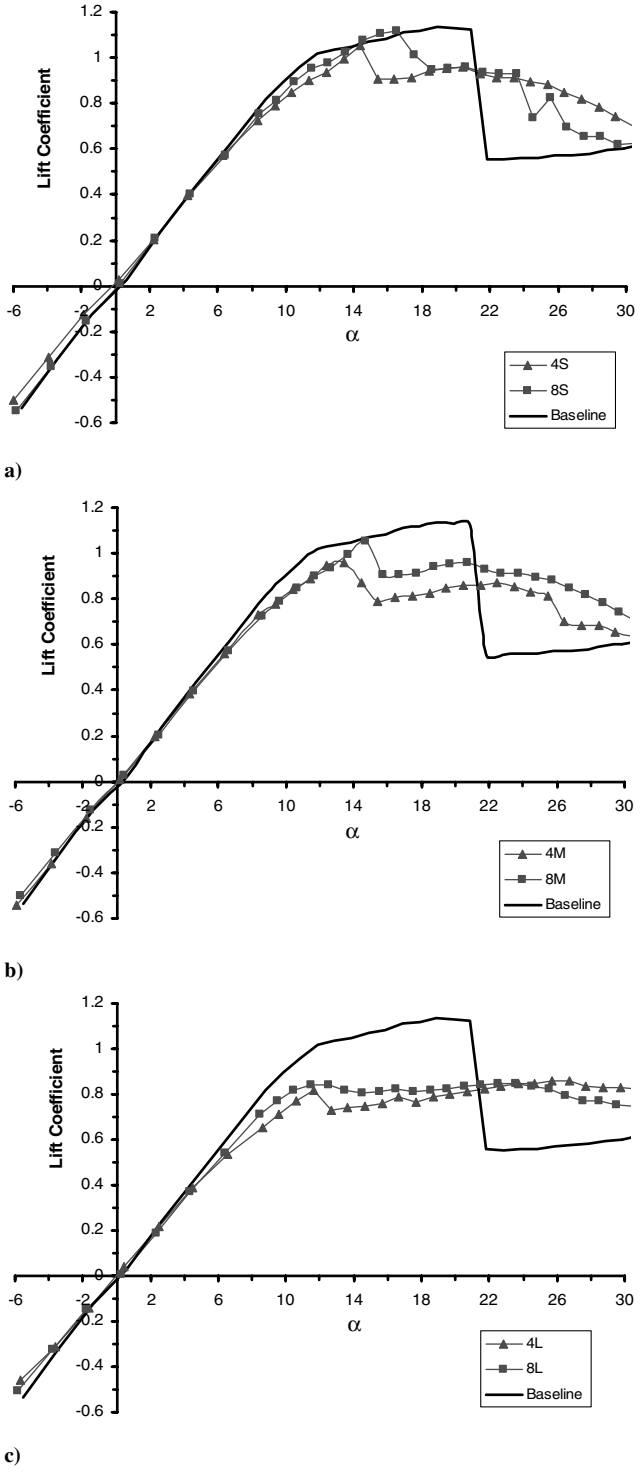

Fig. 6 Dependence of lift coefficient on the protuberance wavelength, with amplitudes of a) 0.025*c*, b) 0.05*c*, and c) 0.12*c*.

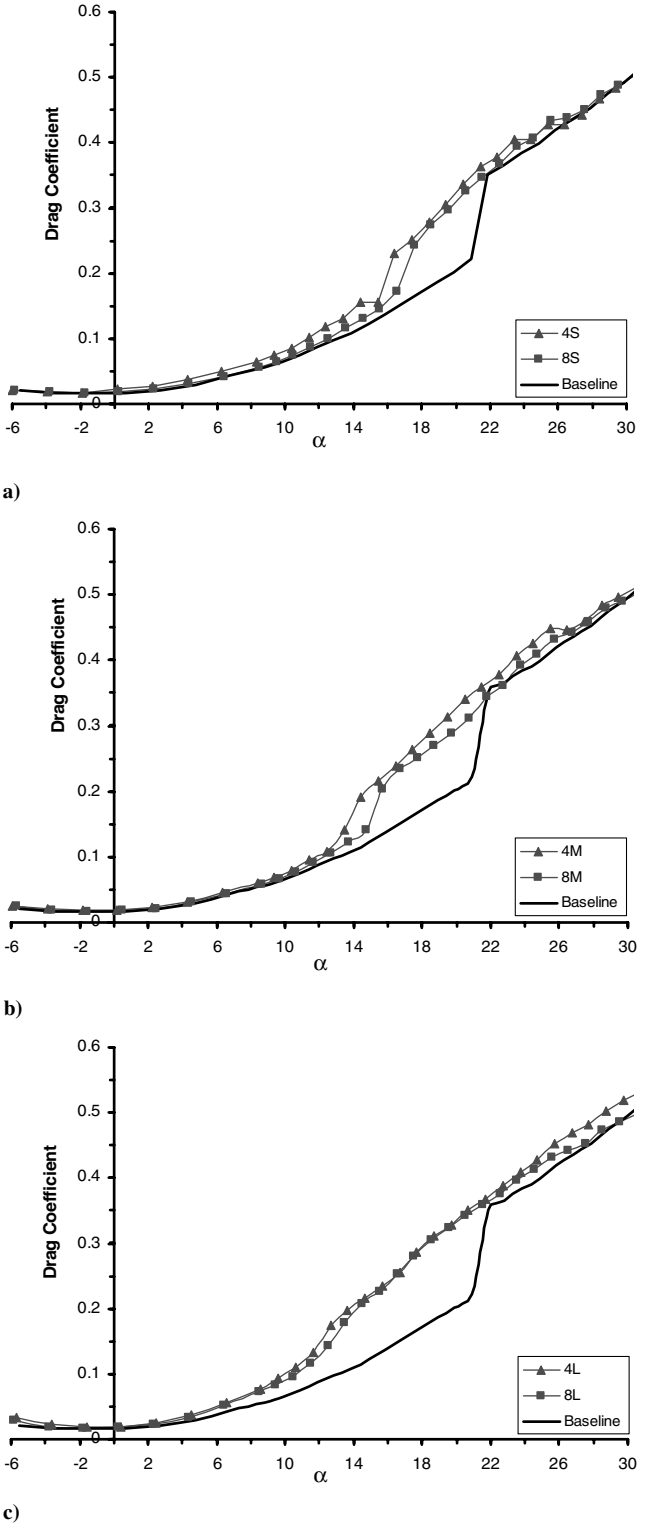

Fig. 7 Dependence of drag coefficient on the protuberance wavelength, with amplitudes of a) 0.025*c*, b) 0.05*c*, and c) 0.12*c*.

amplitude (8M) falls between that of 8S and 8L. At $\alpha \approx 22$ deg, the lift coefficient of the 8M foil is over 50% greater than the C_l for the baseline foil.

The data for the longer wavelength foils shown in Fig. 4b reveal very similar behavior. The C_l for the smallest leading-edge protuberance foil (4S) follows the baseline C_l up to $\alpha \approx 15$ deg before decreasing to a value of $\approx$0.8, and eventually matching the poststall C_l baseline foil at $\alpha \approx 26$ deg. The lift coefficient of the foil with the largest leading-edge protuberances (4L) increases to $C_l \approx 0.8$ and remains fairly constant subsequently (up to $\alpha \approx 30$ deg), analogous to the 8L foil. The intermediate amplitude foil (4M) had C_l values in between those for 4S and 4L throughout the angle-of-attack range.

The aerodynamic characteristics, including the lift curve slope, maximum C_l, angle of maximum C_l, minimum C_d, maximum L/D, angle of maximum L/D, and stall angle, of the foils tested in this study are listed in Table 1. The slope of lift curve, $dC_l/d\alpha$, was measured within the linear range for all the foils. With the exception of the 4S foil, all of the foils with leading-edge protuberances had lower-lift coefficient slopes than the baseline foil. Moreover, $dC_l/d\alpha$ decreases with the protuberances amplitude for both wavelengths. The lowest lift curve slope of 0.081 (per degree) was found for the 4L foil (0.5c wavelength and 0.12c amplitude). The $dC_l/d\alpha$ values in

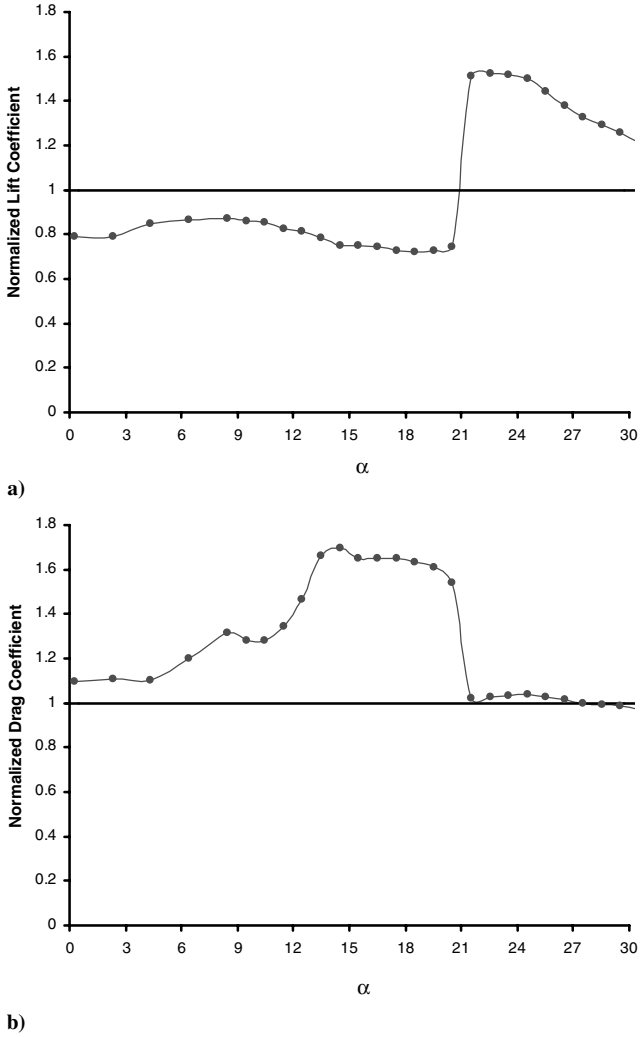

Fig. 8 The 8L foil normalized by the baseline values: a) lift and b) drag.

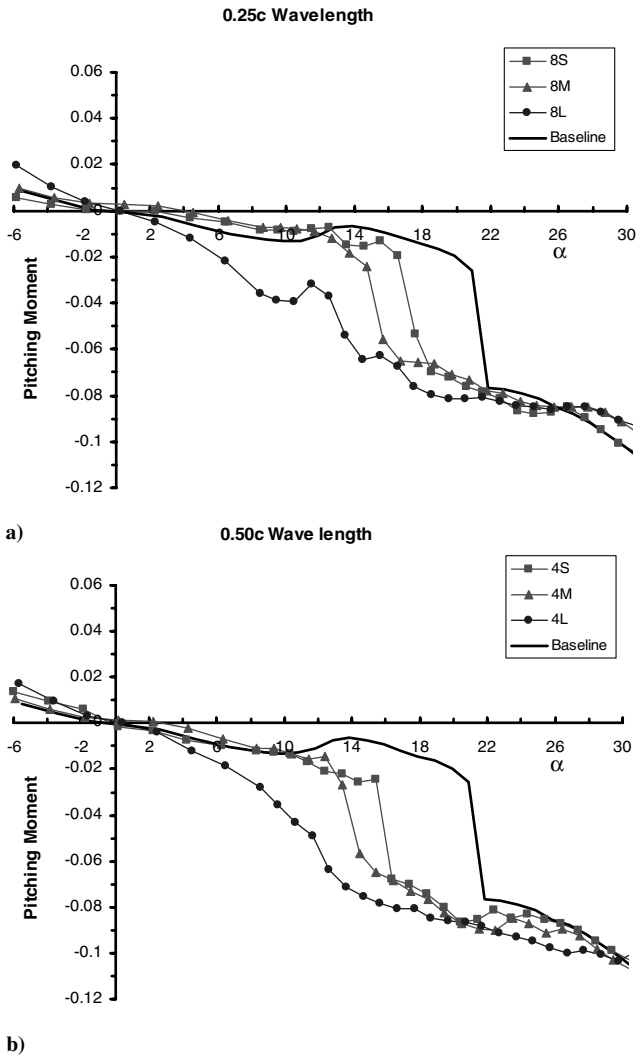

Fig. 9 Pitching moment coefficient variation with angle of attack.

Table 1 may be compared with the potential flow value of 0.11 per degree for ideal two-dimensional thin airfoils. The stall angle for the 8L and 4L foils is not listed in Table 1 as they did not stall in the traditional manner.

The drag coefficient C_d is plotted in Figs. 5a and 5b for the shorter ($0.25c$) and longer ($0.5c$) wavelength airfoils, respectively. The baseline foil had C_d values equal to or smaller than all of the foils with leading-edge protuberances. The largest C_d values at any angle of attack belong to the largest amplitude protuberance foils (4L and 4M). The drag coefficients of foils with leading-edge protuberances in the linear regime (i.e., constant $dC_l/d\alpha$) and for $\alpha > 22$ deg were quite close to the baseline airfoil. In the range of $10 < \alpha < 22$ deg, the airfoils with leading-edge protuberances have greater drag coefficients than the baseline by varying degrees. The C_d in the poststall regime is almost independent of the leading-edge geometry because, at sufficiently large angles of attack, all foils appear to be bluff. Consequently, airfoils with leading-edge protuberances produce larger (by as much as 50%) lift-to-drag ratios than the baseline foil in the poststall regime.

B. Effect of Wavelength

The lift coefficients for the two leading-edge protuberance wavelengths are compared in Fig. 6 for the three amplitudes. In general, the differences between the two wavelengths are small. For example, the lift coefficients for the largest amplitude foils, 4L and 8L, differ by no more than 10% except at $\alpha \approx 13$ deg. For the smallest protuberance amplitude foils, the larger wavelength (4S) causes the angle of maximum C_l to drop by 2 deg. For the intermediate amplitude foils, the angle of maximum C_l for the larger wavelength foil (4M) is about 1 deg less than that of the smaller wavelength foil (8M).

The drag coefficient for the two protuberance wavelengths are contrasted in Fig. 7. Similar to the lift coefficient trend, the effects of protuberance wavelength variation are minor. Nonetheless, it appears that the foils with shorter wavelength protuberances generate slightly less drag than the longer wavelength foils over the majority of angles of attack examined. The effect of wavelength on drag coefficient is observed to be greater for the intermediate protuberance amplitude of $0.5c$ than the other two amplitudes.

In Fig. 8, the lift and drag of the 8L foil normalized by those of the baseline foil is plotted against angle of attack. It is readily seen that at angles below which the baseline foil stalls, the 8L foil has up to 70% higher drag and approximately 20% reduced lift, whereas beyond the baseline stall angle (~21 deg), the 8L foil shows little or no drag penalty (<4%) and a substantial (up to 50%) relative increase of lift force.

C. Pitching Moment

The pitching moment coefficient C_m referenced to the quarter-chord location is plotted in Fig. 9 for all of the airfoils tested. The moment coefficients for the two smaller amplitude protuberance foils (4S and 8S) are generally quite close to the values for the baseline foil up to $\alpha \approx 10$ deg. The baseline foil has a smaller value of pitching moment than the foils with the leading-edge protuberances up to its stall angle of attack. The pitching moments in the poststall regime are nearly comparable for all the airfoils. The two foils with the largest protuberance amplitudes (4L and 8L) have the largest pitching

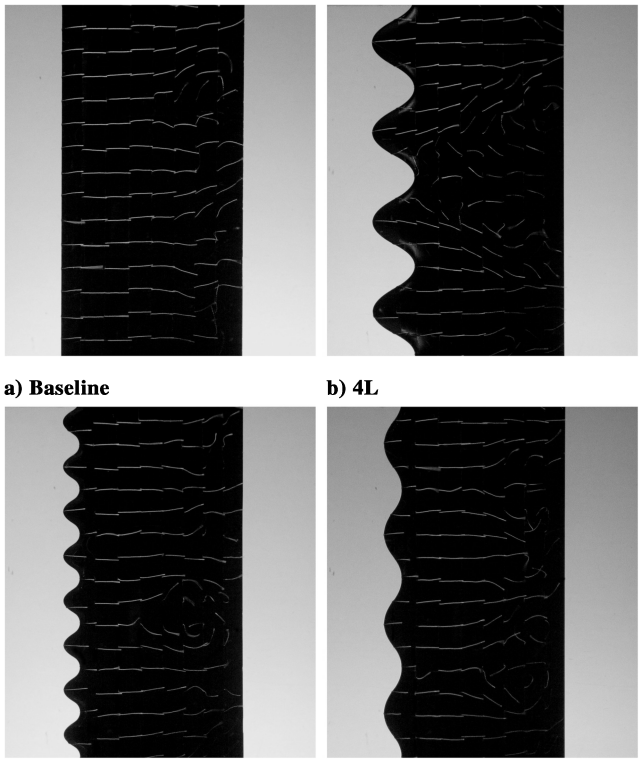

a) Baseline b) 4L

c) 4M d) 8M

Fig. 10 Photographs of airfoils at 12 deg angle of attack.

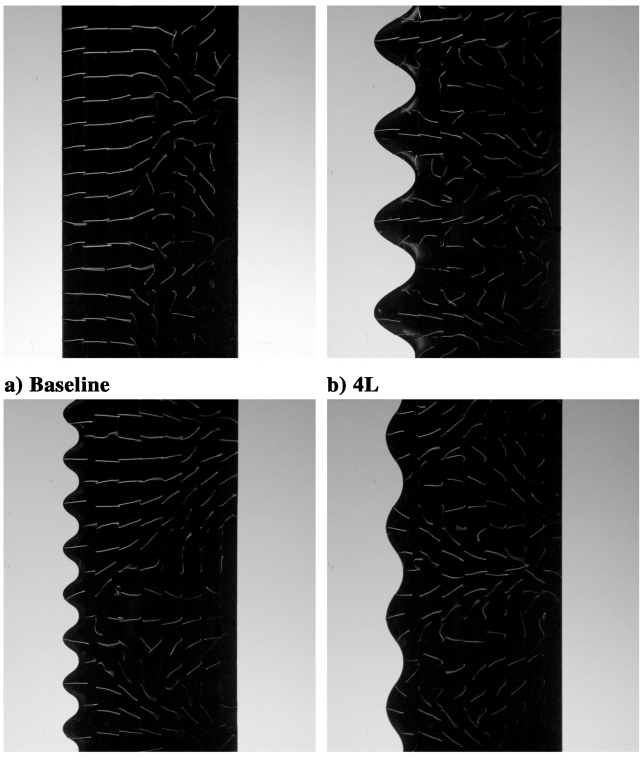

a) Baseline b) 4L

c) 4M d) 8M

Fig. 11 Photographs of airfoils at 18 deg angle of attack.

moment throughout the angle-of-attack range investigated. The larger, compared with the baseline, negative pitching moments observed for the 4L and 8L foils, stems from the prematurely reduced lift in the prestall regime. The significant increase of pitching moment will have an impact on the design of systems employing airfoils with protuberances.

D. Flow Visualization

To assess the state of the flow near the surface, the set with the larger span ($s = 305$ mm) foil was employed. The foils in this set consist of the baseline, 8M, 4M, and 4L. Instantaneous images of surface tufts at $\alpha = 12$, 18, and 24 deg are presented in Figs. 10–12, respectively. The images in these figures show only the central two-thirds of the foil. These specific attack angles were chosen because $\alpha = 12$ deg is after the point at which the largest protuberance amplitude foil deviates from the baseline trend. The other two angles refer to conditions just before and after the baseline foil stalls.

The tufts on the baseline foil at $\alpha = 12$ deg in Fig. 10 show that flow over the first three-quarters of the foil is attached, and only near the trailing edge is the flow separated. In contrast, the flow over half of the foils with leading-edge protuberances seems to be separated, as indicated by the irregular and undulating patterns of surface tufts. Detailed examination of movies and numerous still images similar to those in Fig. 10 reveals that separation appears to originate primarily from the "troughs" in between adjacent protuberances. This is evident in the image of the 4L foil, which has the largest separated flow region among the four foils at $\alpha = 12$ deg. Even though the still image in Fig. 10 indicates a large stall cell in the middle of the 4L foil, there were multiple stall cells starting from other troughs at other instances. The patterns of stall cells shown in Figs. 10–12 were not static and changed with time. Irrespective of such variations, the separation regions appear to initiate mainly from the troughs of foils and the flow remains attached to the protuberance peaks. The baseline foil had the smallest area of separated flow at $\alpha = 12$ deg. The observed extent of the separated flow region correlates well with the lift coefficient data presented earlier.

Increasing the angle of attack to $\alpha = 18$ deg results in the separation line moving up to about $0.5c$ on the baseline foil, as indicated by the last 4–5 rows of tufts in Fig. 11. For the largest amplitude protuberance foil, flow separation is observed over three-quarters of the foil and in the trough regions. The intermediate amplitude foil 4M has a tuft pattern similar to that of 4L. However, the 8M foil has a larger attached flow area. Again, the difference between the 4M and 8M foils corresponds directly to the lift coefficient values at $\alpha = 18$ deg.

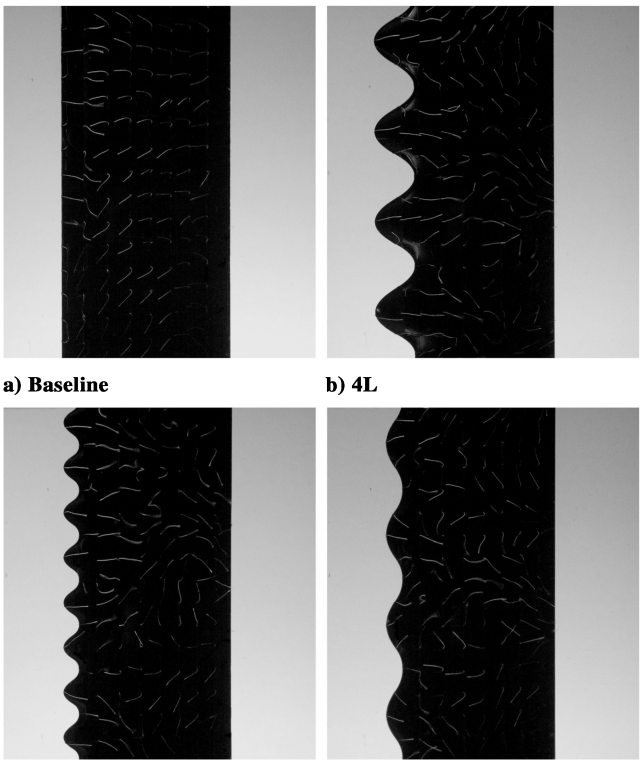

a) Baseline b) 4L

c) 4M d) 8M

Fig. 12 Photographs of airfoils at 24 deg angle of attack.

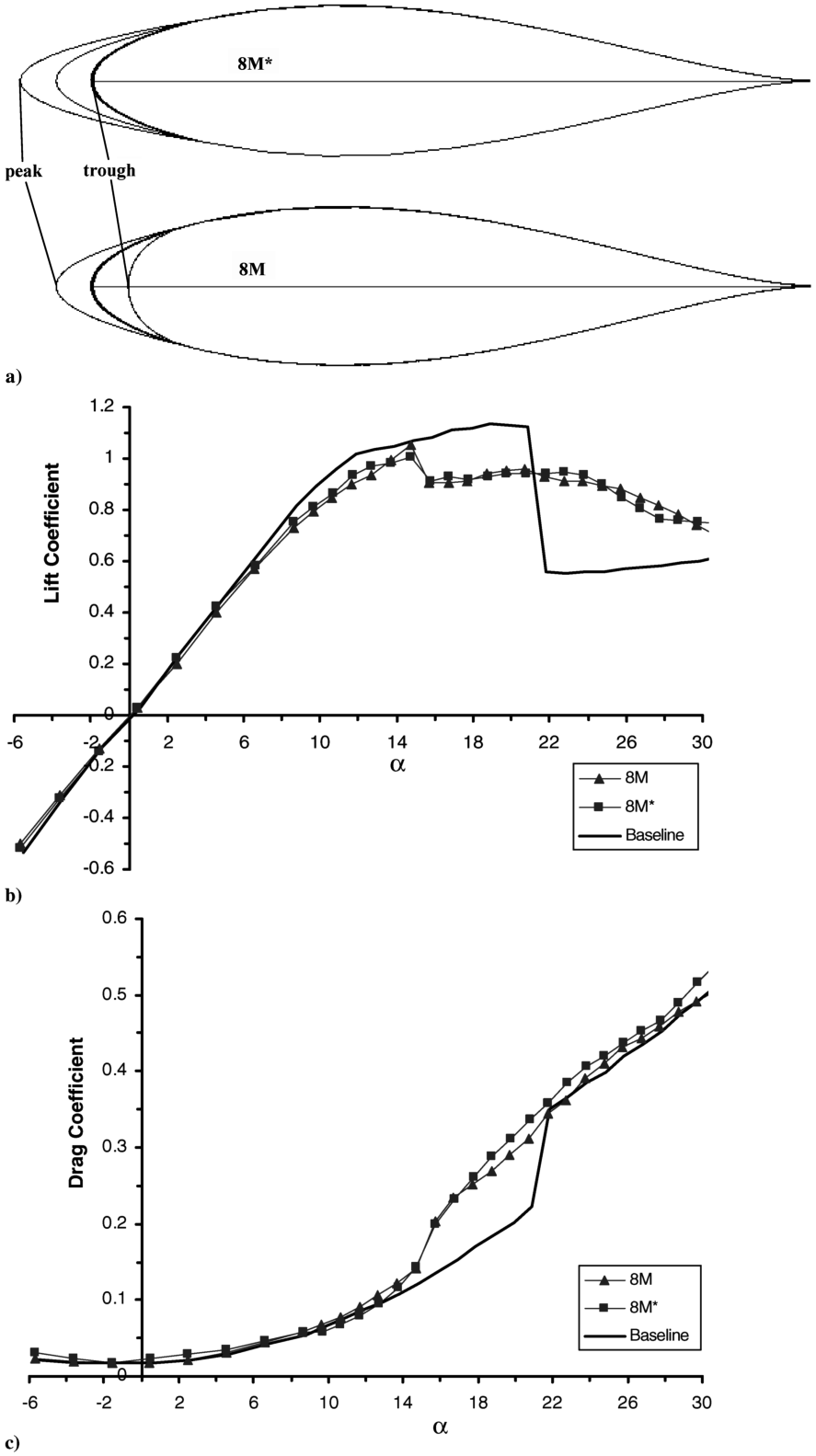

Fig. 13 Comparison of 8M and 8M* foils with different leading-edge geometry: a) schematics of the foil profiles, b) lift coefficients, and c) drag coefficients.

In the poststall regime at $\alpha = 24$ deg, the flow over the entire baseline foil is separated. Significant flow reversal is present over the majority of the baseline foil surface in Fig. 12. On the other hand, the flow over the leading-edge protuberances remains attached even though the flow over the rest of the airfoil is fully separated. This is clearly visible in the 4L foil image. The tuft pattern over the 4L foil is nearly unchanged between $\alpha = 18$ and 24 deg, corroborating the nearly constant C_l over this angle-of-attack range. Moreover, the presence of attached flow over the protuberance surfaces in the poststall regime ensures that the lift coefficient for the foils with leading-edge protuberances is greater than that for the fully stalled baseline foil.

E. Leading-Edge Geometry

A possible reason for the premature appearance of flow separation in the troughs between adjacent protuberances at relatively small angles of attack could be the blunter leading-edge radius of curvature compared with the baseline foil or the "peak" regions. To investigate the effect of leading-edge geometry, and specifically the leading-edge radius, on the aerodynamic coefficients, another foil (designated 8M*) with leading-edge protuberance amplitude and wavelength comparable to the 8M foil was designed and fabricated. The 8M* foil cross section at three spanwise locations corresponding to the peak, middle, and trough of the protuberance is shown in Fig. 13a. The baseline NACA 63_4-021 profile is indicated by the bold curve. Even though the leading edge of the 8M* foil has a sinusoidal profile, the largest leading-edge radius (in the trough region) is equal to that of the baseline foil. The profile for the peak cross section has a smaller leading-edge radius. The profile of the 8M foil is also shown in Fig. 13a, in which the trough profile has quite a large leading-edge radius. The profiles of all three foils past the $0.4c$ chord location are identical.

The lift and drag coefficients for the two foils 8M and 8M* with $0.05c$ amplitude and $0.25c$ wavelength protuberances are presented in Figs. 13b and 13c, respectively. The C_l data indicate that there is very little difference (less than about 5%) between the two foils. Drag coefficients for the two foils have a similar trend, with a slightly larger drag associated with the 8M* foil for $\alpha > 18$ deg. Thus, it appears that the leading-edge geometry, at least for the foils with the sinusoidal leading edge, does not play a major role in the aerodynamic characteristics of the foil over the range of angles of attack studied. The primary reason for the observed aerodynamic loading of foils with protuberances appears to be the modification of the flow separation pattern over the protruded regions of the leading edge.

IV. Discussion

The two-dimensional airfoil with leading-edge protuberances tested by Stein and Murray [6] at angles of attack up to $\alpha = 12$ deg is the closest work to the one presented here. Although the wavelength and amplitude of the airfoil tested in [6] does not match any of the ones tested here, the lift and drag coefficient behavior are qualitatively similar to the $0.25c$ wavelength foils in the present experiments. On the other hand, the effect of protuberances on the three-dimensional models of whale flippers tested in [5] is quite different. The flipper model with protuberances had reduced drag in the poststall regime and the stall angle was extended beyond the baseline flipper. It may be argued that the presence of protuberances affects the induced drag and the spanwise progression of stall on the three-dimensional flipper model.

An application of the present findings would be in foils designed with an actively controlled leading edge. In the prestall regime, the airfoil leading edge would be free of any protuberances. As the airfoil angle of attack approaches the stall angle, actuators at the leading edge will be activated to generate protuberances of appropriate amplitude at the leading edge. The foil will now have load characteristics of the modified cases in the poststall regime. In this manner, the performance of the foil in both the prestall and poststall regimes could be optimized. Systems with airfoils operating beyond the stall regime could possibly benefit from such an active system.

V. Conclusions

The effects of sinusoidal protuberances on the leading edge of nominally two-dimensional NACA 63_4-021 airfoils were examined experimentally in a series of water-tunnel tests. The amplitude of leading-edge protuberances ranged from 2.5 to 12% of the mean chord length, with spanwise wavelengths of 25 and 50% of the mean chord length. The ranges of protuberance amplitude and wavelength correspond to those found on the leading edge of a humpback whale's flipper. The lift, drag, and pitching moment coefficients were computed from the measured load data. The following conclusions are drawn from the measurements:

1) The foils with the leading-edge protuberances did not stall in the same manner as the baseline foil with the smooth leading edge. The protuberances caused a reduction in the lift coefficient at angles of attack below the baseline foil stall angle. In the poststall regime, the airfoils with protuberances had higher lift coefficients, by as much as 50%, over the baseline foil. The lift coefficient for the largest amplitude protuberances was nearly constant for the range of $10 < \alpha < 26$ deg.

2) The foils with protuberances had greater drag coefficients in the prestall regime; however, the drag was nearly independent of the leading-edge geometry in the poststall regime. The lift-to-drag ratio in the poststall regime could be increased substantially with the protuberances.

3) For the foils tested, the wavelength of protuberances and the leading-edge radius played a minor role on the force and moment coefficients. On the other hand, the protuberance amplitude had a significant effect on the resulting forces and moments.

4) Flow visualization using surface tufts revealed that the flow over the protuberances remained attached well past the angle of attack where the baseline airfoil stalls. On the other hand, flow separation at the leading edge of modified foils occurred mainly in the troughs between the adjacent protuberances. The wavelength of the protuberances had a minor effect on the flow separation.

The quantitative details of the flowfield and the mechanisms for the observed tuft patterns will be examined in future work.

Acknowledgments

This project has been supported by the Office of Naval Research, University-Laboratory Initiative program through contract N00014-05-1-0306 at Worcester Polytechnic Institute and contract N00014-05-WX-2-0676 at the Naval Undersea Warfare Center. Useful discussions with Frank Fish are greatly appreciated. The efforts of Worcester Polytechnic Institute Haas Center personnel with the fabrication of the airfoils are acknowledged.

References

[1] Fish, F. E., and Battle, J. M., "Hydrodynamic Design of the Humpback Whale Flipper," *Journal of Morphology*, Vol. 225, July 1995, pp. 51–60. doi:10.1002/jmor.1052250105

[2] Fish, F. E., "Performance Constraints on the Maneuverability of Flexible and Rigid Biological Systems," *Proceedings of the Eleventh International Symposium on Unmanned Untethered Submersible Technology (UUST), UUST99*, Autonomous Undersea Systems Inst., Lee, NH, Aug. 1999, pp. 394–406.

[3] Bushnell, D. M., and Moore, K. J., "Drag Reduction in Nature," *Annual Review of Fluid Mechanics*, Vol. 23, Jan. 1991, pp. 65–79. doi:10.1146/annurev.fl.23.010191.000433

[4] Watts, P., and Fish, F. E., "The Influence of Passive, Leading Edge Tubercles on Wing Performance," *Proceedings of the Twelfth International Symposium on Unmanned Untethered Submersible Technology (UUST), UUST01*, Autonomous Undersea Systems Inst., Lee, NH, Aug. 2001.

[5] Miklosovic, D. S., Murray, M. M., Howle, L. E., and Fish, F. E., "Leading-Edge Tubercles Delay Stall on Humpback Whale (*Megaptera novaeangliae*) Flippers," *Physics of Fluids*, Vol. 16, No. 5, May 2004, pp. L39–42. doi:10.1063/1.1688341

[6] Stein, B., and Murray, M. M., "Stall Mechanism Analysis of Humpback Whale Flipper Models," *Proceedings of Unmanned Untethered Submersible Technology (UUST), UUST05*, Autonomous Undersea Systems Inst., Lee, NH, Aug. 2005.

[7] Murray, M. M., Miklosovic, D. S., Fish, F. E., and Howle, L., "Effects of Leading Edge Tubercles on a Representative Whale Flipper Model at Various Sweep Angles," *Proceedings of Unmanned Untethered Submersible Technology (UUST), UUST05*, Autonomous Undersea Systems Inst., Lee, NH, Aug. 2005.

[8] Naumann, A., Morsbach, M., and Kramer, C., "The Conditions of Separation and Vortex Formation Past Cylinders,"*AGARD Conference Proceedings No. 4, Separated Flows*, AGARD CP 4, Pt. 2, 1966, pp. 539–574.

[9] Tanner, M., "A Method of Reducing the Base Drag of Wings with Blunt Trailing Edges," *Aeronautical Quarterly*, Vol. 23, Dec. 1972, pp. 15–23.

[10] Bearman, P. W., and Tombazis, N., "Effect of Three-Dimensional Imposed Disturbances on Bluff Body Near Wake Flows," *Journal of Wind Engineering and Industrial Aerodynamics*, Vol. 49, Dec. 1993, pp. 339–350. doi:10.1016/0167-6105(93)90029-N

[11] Tombazis, N., and Bearman, P. W., "A Study of Three-Dimensional Aspects of Vortex Shedding from a Bluff Body with a Mild Geometric Disturbances," *Journal of Fluid Mechanics*, Vol. 330, Jan. 1997, pp. 85–112. doi:10.1017/S0022112096003631

[12] Bearman, P. W., and Owen, J. C., "Reduction of Bluff-Body Drag and Suppression of Vortex Shedding by the Introduction of Way Separation Lines," *Journal of Fluids and Structures*, Vol. 12, Jan. 1998, pp. 123–130. doi:10.1006/jfls.1997.0128

[13] Pope, A., and Ray, W. H., "*Low-Speed Wind Tunnel Testing*," 2nd ed., Wiley, New York, 1984.

F. Coton
Associate Editor